Monthly Notices
of the
ROYAL ASTRONOMICAL SOCIETY

MNRAS **469,** 3564–3575 (2017)
Advance Access publication 2017 April 28

doi:10.1093/mnras/stx1009

Two regimes of galaxy dynamics: mass models of NGC 5055 and DDO 154

Milena Jovanović★

Astronomical Observatory of Belgrade, Volgina 7, 11060 Belgrade, Serbia

Accepted 2017 April 25. Received 2017 April 25; in original form 2016 November 4

ABSTRACT

We derive detailed dynamical models for two galaxies, the massive spiral galaxy NGC 5055 and the dwarf irregular DDO 154. We used Navarro, Frenk & White (NFW) and isothermal halo models for the dark matter (DM) distribution, along with the most recent and reliable radio observations of H I to determine the rotation curves of these galaxies. Contributions from the neutral gas and the luminous matter were accounted for. For NGC 5055, the latest stellar population synthesis (SPS) models, combining metallicity and age as indicators of the stellar mass-to-light ratio (M/L) were used to better constrain both the DM model and the contribution to the total mass from all components. The isothermal dark halo model successfully fitted both observed rotation curves with realistic values for stellar M/L, while the NFW model needed further constraints for M/L to fit the rotation curve of DDO 154. In the case of NGC 5055, we found the best-fitting M/L in the 3.6 μm band ($M/L_{3.6}$) for stellar disc to be 0.57 ± 0.04 for isothermal, and 0.50 ± 0.05 for NFW DM model. The most probable value for $M/L_{3.6}$ from SPS models is 0.46, which is in agreement within uncertainties with our best-fitting NFW model. In the case of DDO 154, we obtained the stellar disc $M/L_{3.6}$ of 0.25 ± 0.20 for the isothermal DM model. The stellar disc $M/L_{3.6}$ for the NFW model was fixed to 0.26, as best reasonable value. For NGC 5055, we derived radial profiles of stellar M/L for our best estimate for a particular DM model.

Key words: galaxies: dwarf – galaxies: spiral – galaxies: structure – dark matter.

1 INTRODUCTION

The key factor in understanding the dynamics and evolution of galaxies is the relation between the baryonic and non-baryonic component of matter that we find associated with every galaxy, as well as the various forms in which we observe this baryonic matter. Indirectly, this gives us information on how and when galaxies form, along with other structures, which is of great cosmological importance. Subsequent evolution leaves imprint on the distribution of baryons over different galactic components, as well as over different forms (collapsed stellar objects and various gaseous phases).

Baryonic mass function (BMF) is usually defined as the number density of galaxies as a function of their baryonic mass. BMF is constructed as a sum of all the various visible components of baryonic matter, such as stellar component, and atomic and molecular gas (Salucci & Persic 1999; Bell et al. 2003; Read & Trentham 2005). From the BMF, we get the total amount of baryons residing in all galaxies, which is, as is found previously, in strong discrepancy with baryonic matter census from big bang nucleosyntheses - the so-called missing baryon problem. By comparing baryonic component with total dynamical mass, we can get the baryon fraction, and its dependence on the total halo mass. This, in turn, enables putting tighter constraints on the scenarios for galaxy formation and evolution, notably controversial issues, such as baryonic blow-out, efficient supernova feedback, late infall, or bulge formation (e.g. Baugh 2006).

It is possible to construct the BMF for a sample of H I selected local galaxies, for which the high-resolution rotational curves (RCs) are available. From them good and detailed dynamical models can be inferred. This would provide us with a small, yet reliable, sample for possible comparison with high-redshift systems, and testing of the possibility of late-stage incorporation of gas, which we expect to be confined in mini-clouds in the galaxy halo and unavailable to observation (Rees & Ostriker 1977; Fukugita, Hogan & Peebles 1998; Salucci & Persic 1999). Comparison with a larger or optically selected BMF from a statistically significant sample is also possible (Papastergis et al. 2012; Papastergis 2013).

Here, we are presenting a test study on the two galaxies that we have reason to believe are probing two of the extremes of the nearby galaxy mass distribution. Previous studies found them to have a very different stellar and halo mass, and, from that, baryonic fraction and the behaviour of the 'baryon retention fraction' (ability of the galaxy to retain the amount of incorporated baryons as a function of the host halo mass). Detailed dynamical models for two galaxies, massive spiral galaxy NGC 5055 and dwarf irregular

★E-mail: milena@aob.bg.ac.rs

© 2017 The Author
Published by Oxford University Press on behalf of the Royal Astronomical Society

Downloaded from https://academic.oup.com/mnras/article/469/3/3564/3779716 by Access provided by HEAL-Link (University of Athens) user on 12 December 2022

DDO 154 are presented as case studies for the two dynamical regimes. We used Navarro, Frenk & White (NFW) and isothermal halo (ISO) models for the dark matter (DM) distribution and THINGS[1] survey observations of H I in determining the RCs of these galaxies (Walter et al. 2008). THINGS data were also used to infer the contribution from the neutral gas. For assessing the mass of the luminous matter, we used observations from the *Spitzer* Survey of Stellar Structure in Galaxies (S4G, Sheth et al. 2010).[2] The two tested models can both fit the observed RC reasonably well. The latest stellar population synthesis (SPS) models combining metallicity and age as indicators of the stellar mass-to-light ratio (M/L) in the case of NGC 5055, were used to better constrain $M/L_{3.6}$ of the stellar component and thereby, the 'best' DM model. For NGC 5055, we derived radial profiles of stellar M/L for our best estimate of a particular DM model. The overall contribution of the baryon mass to the total inferred dynamical mass derived from our best-fitting models is discussed in the context of the BMF of galaxies.

Clearly, the procedure cannot account sufficiently well for the baryonic mass in haloes at large galactocentric distances, since the most distant data points are still too close in comparison to the independently established extent of haloes. Such independent data come, for instance, from dynamical or Lyα absorption correlations studies (Lanzetta et al. 1995; Churchill et al. 2015) or OVII absorption observations (Miller, Hodges-Kluck & Bregman 2016).

The plan of the paper is as follows: in Section 2, we introduce the observational data and the extraction of parameters used in our modelling procedure. Section 3 describes the dynamical mass models and the SPS models. Results of the modelling are given in Section 4. The discussion, conclusions, and directions for further work are given in Sections 5 and 6.

2 OBSERVATIONAL DATA AND METHODS

All the data come from publicly available sources and they are appropriately quoted. We decided to derive observational quantities that we use in our models wherever we found it possible, in order to obtain the most reliable values based on the latest observational and theoretical approaches.

2.1 Photometric observations

3.6 μm images of NGC 5055 and DDO 154 from the S4G (Sheth et al. 2010) are used in obtaining the dynamical mass of the stellar component. S4G is a deep infrared (IR) imaging survey of nearby galaxies. IR bands are convenient for the present purpose, since they avoid both internal and Galactic extinction. Internal extinction may be completely neglected in the mid-IR (Draine & Lee 1984), and the Galactic extinction is low as well. M/L in near-IR (NIR) bands is affected by dust and young stars to a lesser extent than in the optical but still depends on metallicity, star formation history (SFH), and especially the age of the population. Deep imaging in mid-IR bands traces old stars, with the effects of dust extinction and star formation activity less pronounced compared to ground-based images in both optical or NIR band (e.g. Meidt et al. 2014). *Spitzer* 3.6 μm band is considered as one of the best tracers of the stellar mass (Pahre et al. 2004).

We use the images from the S4G (see footnote above) survey, that have already been processed through the Pipeline 1, creating

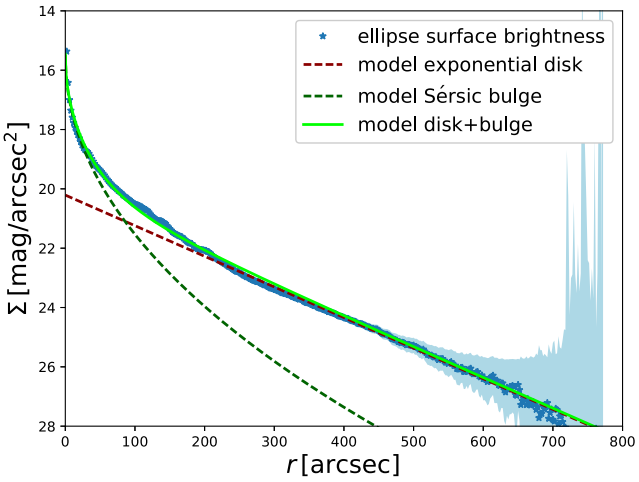

Figure 1. Surface brightness of NGC 5055 measured by `ellipse` task (blue stars) with uncertainties (light blue region) and adopted GALFIT model components – exponential disc (red dashed line), Sérsic bulge (dark green dashed line), and total modelled disc+bulge (light green full line).

science-ready mosaics from the original images. To perform the decomposition of the 3.6 μm image of both galaxies we used the GALFIT code (Peng et al. 2010). Accompanying images necessary to perform our decomposition of the galaxies were obtained from Pipeline 4[3] (Salo et al. 2015). For the surface brightness decomposition, we need a bad pixel mask, containing frames that are masking the foreground/background objects and various image defects. Pipeline 4[4] provides the edited masks which we used (made from automatically created ones in Pipeline 2, Muñoz-Mateos et al. 2015), and also the sky background estimates and the ellipse fits. The latter determine the position of the galaxies' centres and the orientation of each galaxy relative to the sky plane, estimated from the shape of the galaxy's outer isophotes. The necessary σ and point spread function images are provided with detailed descriptions and recommended for use if re-running the decomposition, which we did.

While the best human-supervised decomposition of NGC 5055 provided by Salo et al. (2015), consisted of a nucleus and two exponential discs, we decided on the classical bulge and disc decomposition. Because we wanted to improve the constraint on the outer parts of the surface brightness profile, we first fitted the outer component, the exponential disc, from one-dimensional (1D) surface brightness profile provided as an output of IRAF task `ellipse` as a part of Pipeline 3 (Muñoz-Mateos et al. 2015). Subsequently, we performed the two-dimensional (2D) fitted with GALFIT, while keeping the parameters for the disc fixed (or, more precisely, varied around the 1D parameter solution). With this approach, our decomposition becomes of comparable quality to the one in Salo et al. (2015), while keeping the modelling of the outer parts of the galaxy's light profile robust. In Fig. 1, we show how the model that is the result of our 2D fit (bulge + disc) corresponds to 1D surface brightness profile, measured by IRAF `ellipse` task in Pipeline 3. The best-fitting parameters are given in Table 1.

For the DDO 154, best-fitting decomposition of the observed surface brightness in 3.6 μm image, we were satisfied with a one

[1] Available at: http://www.mpia.de/THINGS
[2] Available at: http://irsa.ipac.caltech.edu/data/SPITZER/SINGS/galaxies
[3] Available at: http://www.oulu.fi/astronomy/S4G_PIPELINE4/MAIN
[4] Pipeline 5 images based on Querejeta et al. (2015) would be preferable, but they are not available for the two analysed galaxies.

Downloaded from https://academic.oup.com/mnras/article/469/3/3564/3779716 by Access provided by HEAL-Link (University of Athens) user on 12 December 2022

Table 1. GALFIT parameters for stellar components of NGC 5055 and DDO 154, as well as our adopted parameters describing the gas disc: μ_s – surface brightness for the exponential disc and r_s – corresponding disc scale radius in angular size units; μ_e – surface brightness for the Sérsic bulge and r_e – corresponding effective radius; n – index for Sérsic bulge fit (only in the case of NGC 5055), z_0 – scaleheight of the model stellar exponential disc, and z_0^{gas} – scaleheight of the model gaseous exponential disc.

Galaxy ID	μ_s(mag arcsec^{-2})	r_s(arcsec)	μ_e(mag arcsec^{-2})	r_e(arcsec)	$n_{Sèrsic}$	z_0(kpc)	z_0^{gas}(kpc)
NGC 5055	20.210	105.22	19.586	45.00	2.059	0.917	0.200
DDO 154	14.817	26.54	–	–	–	0.100	0.708

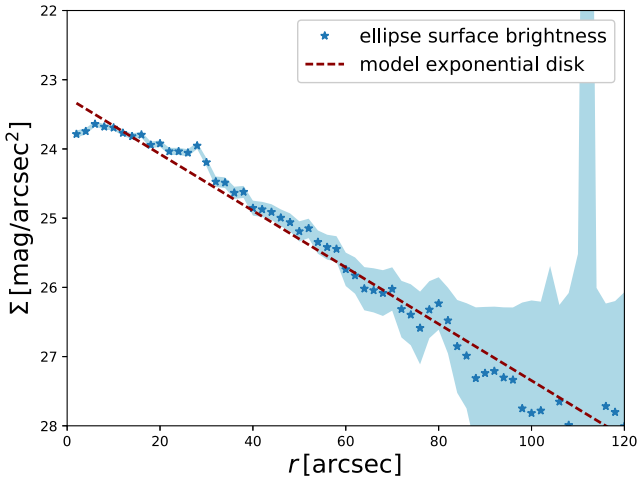

Figure 2. Surface brightness of DDO 154 measured by `ellipse` task (blue stars) with uncertainties (light blue region) and adopted GALFIT model exponential disc (red dashed line).

component exponential disc, with parameters of the fitted very close to the one provided by Salo et al. (2015). In Fig. 2, we show the comparison to surface brightness 1D profile, similar to Fig. 1. Again, the corresponding best-fitting parameters are given in Table 1.

The fitted parameters obtained using GALFIT that are shown in Table 1 are used in our dynamical models in Section 3.

2.2 Radio observations

Radio data used in this paper are all based on THINGS survey data release.

2.2.1 *Gas contribution*

Mass density profiles of atomic gas in the two galaxies in question are based on THINGS integrated H I maps. The Groningen Image Processing System (GIPSY)[5] task `ellint` was used in fitting tilted rings to the naturally weighted first moment maps, with values for position angle (PA) and inclination (i) fixed. Values for PA and i are the median values of their radial profiles derived using GIPSY task `rotcur` with those two parameters left free (see Section 2.2.2). Median values for PA and i that we use are PA $= 100.9^\circ$ and $i = 60^\circ$, for NGC 5055, and PA $= 225.5^\circ$ and $i = 65^\circ$ for DDO 154, and we list them in Table 2. The above-mentioned parameters describe the geometry of a well-defined gas disc. In Table 2, we are giving the values for i of a stellar disc from HyperLeda[6] and previously found i of gas disc from de Blok et al. (2008) for comparison.

To convert from integrated intensity to mass density distribution, we used the expression from Leroy et al. (2008):

$$\Sigma_{\rm H\,I}({\rm M}_\odot{\rm pc}^{-2}) = 0.020 \cos i\, {\rm I}_{\rm 21cm}({\rm K\ km\ s}^{-1}), \quad (1)$$

which accounts for the presence of helium (factor of 1.36) and the i. Molecular gas was omitted from the calculation at this point.

2.2.2 *Rotation curves*

For both NGC 5055 and DDO 154, we derive the RCs from the THINGS data cubes, closely based on de Blok et al. (2008).

The RCs are derived through a tilted-ring fitting to the 2D velocity map, using GIPSY task `rotcur`. For the type of velocity map that we use to perform the tilted-ring analysis, we decided on the Gauss–Hermite h_3 polynomial fitted to the observed velocity profiles. Gauss–Hermite h_3 polynomial (van der Marel & Franx 1993) is known to be effective in modelling skewness of the observed velocity profiles with significant asymmetries. Hermite h_3 polynomials give more stable results, even for low signal-to-noise (S/N) profiles compared to different types of velocity maps (e.g. first moment map, peak velocity fields, and single Gaussian, see Oh et al. 2011). We used another GIPSY task, `xgaufit` to fitted h_3 polynomial to the observed velocity profile at each pixel (position on the sky). The centre of this asymmetric Gauss–Hermite profile was then assigned to each position on the sky, leaving us with the velocity map for further analysis. Similar constraints as in de Blok et al. (2008) regarding the strength of the observed signal and dispersion were applied, so only the profiles that had fitted maximums higher than $3\sigma_{\rm chan}$ and dispersions larger than channel separation (parameters taken from Walter et al. 2008) were used. As an additional mask, we used the zeroth moment H I integrated maps and excluded the pixels where there was no measured signal (typical sensitivity limit for THINGS data was 4×10^{19} cm^{-2}, Walter et al. 2008).

Tilted-ring fitting entails that a galaxy's observed projected disc is divided into a set of concentric elliptical rings, with given radii (r) and assumed i, PA, systemic velocities ($V_{\rm sys}$), rotation velocities ($V_{\rm c}$), and centre positions (x_0, y_0). GIPSY task `rotcur` is varying the parameters that describe each 2D elliptical ring using a least-squares algorithm to fit the following expression:

$$V(x, y) = V_{\rm sys} + V_{\rm c}(r) \sin i \cos\theta, \quad (2)$$

until convergence is reached. Phase angle θ is measured in a coordinate system of the galaxy from the receding part of the major axis (see Begeman 1987, for details). Points closer to the major axis are the least affected by projection effects so we use weighing of a fit with $\cos\theta$.

For consistency, all of the initial parameter values are taken from HyperLeda,[7] with value for centre initially set to (0, 0). Again, similar to de Blok et al. (2008), we are running `rotcur` several

[5] https://www.astro.rug.nl/~gipsy
[6] http://leda.univ-lyon1.fr
[7] See footnote 4.

Downloaded from https://academic.oup.com/mnras/article/469/3/3564/3779716 by Access provided by HEAL-Link (University of Athens) user on 12 December 2022

Table 2. Basic parameters describing NGC 5055 and DDO 154: distance from the EDD (see footnote 7) in megaparsecs, PA, and i calculated from GIPSY task `rotcur` in degrees. Inclinations of the H I gas disc from de Blok et al. (2008) ($i_{\rm HIdeBlok}$) and of the stellar disc from HyperLeda ($i_{\rm stellarLEDA}$) are also listed.

Galaxy ID	Morphological type	D (Mpc)	Centre α_{2000}(h m s)	Centre $\delta_{2000}(^\circ\ '\ '')$	PA (°)	i (°)	$i_{\rm HIdeBlok}$ (°)	$i_{\rm stellarLEDA}$ (°)
NGC 5055	Sbc	8.99 ± 0.45	13 15 49.2	42 01 45.3	100.9	60	51	54.9
DDO 154	I	4.04 ± 0.20	12 54 05.9	27 09 09.9	225.5	65	70	56.2

times to put better constraints on parameters other than rotational velocity, i.e. systemic velocity, position of the centre, and PA and i, which are all left as a free parameter in the first run of the fitting procedure. Sampling radius of 5 arcsec was used for both galaxies, given that this is the value that is close to the observational resolution of the radio data in both cases.

In the case of NGC 5055, there are two distinct regions regarding the position of the centre and $V_{\rm sys}$. That is an argument in favour of the outer parts of the galaxy being kinematically decoupled from the core. Relying on the analysis of Battaglia et al. (2006), which is based on the data of similar resolution, we tried moving the centre of rotation to positions that are corresponding to the best-fitting solutions in several observed distinct regions. Such treatment increases the symmetry, but we did not find any improvement in stability of other parameters and no significant effect on the derived rotation velocities (Battaglia et al. 2006, did not find much overall difference between RCs, derived for moving and fixed centres). The best-fitting centre position for the very inner region is close to the one suggested by Battaglia et al. (2006) and also to the value from Trachternach et al. (2008), who looked into centre determination from radio data in great detail. Since we found little evidence for changing the position of the centre, we decided to keep it fixed for the whole galaxy with the value determined in Trachternach et al. (2008). Setting (x_0, y_0) to these values, we are still left with two regions with respect to the change in the systemic velocity. A similar result was found by other authors (Battaglia et al. 2006; de Blok et al. 2008). We adopt the value of $V_{\rm sys} = 496.0\,{\rm km\,s^{-1}}$ for inner 210 arcsec, and $V_{\rm sys} = 504\,{\rm km\,s^{-1}}$ for the outer part. When looking into PA and i, the situation seemed to be more drastic. The changes in these two parameters, especially i, are substantial when moving from inner to outer radii in the case of NGC 5055. Rise in i inside the optical disc obtained by fitting procedure would imply the warped stellar disc, for which there is no evidence in the case of the NGC 5055. The warp is observed in the outer parts which was also found in earlier work (see Battaglia et al. 2006; de Blok et al. 2008). Therefore, for the radial profile of i, we adopted one constant mean value in the inner 700 arcsec, which was $i = 61.25^\circ$. Outer part of i, same as the PA profile, was smoothed, fitted with the appropriate polynomial function, and cleaned out of statistical outliers where needed, to obtain more stable profile. We are thus reducing possible degeneration effects of PA and i on extracting the underlying rotational velocity. Our derived profiles differ from de Blok et al. (2008) and are given in Fig. 3. PA and i strongly affect the derived RC and consequently the fitted mass model.

In estimating the uncertainty of RCs derived as described above, we found that the de Blok et al. (2008) conservatively set limit to be well founded. The uncertainty in any given point was calculated as the sum of velocity dispersion of individual velocity values along one tilted ring ($\sigma_{\rm V}$), and the uncertainty that is due to the difference between the rotational velocities of the approaching ($V_{\rm app}$) and receding side ($V_{\rm rec}$) of the galaxy. We relied on de Blok et al. (2008) and references therein to estimate the uncertainty due to the asymmetry as $1/4 \times (V_{\rm app} - V_{\rm rec})$. When calculating rotational velocities

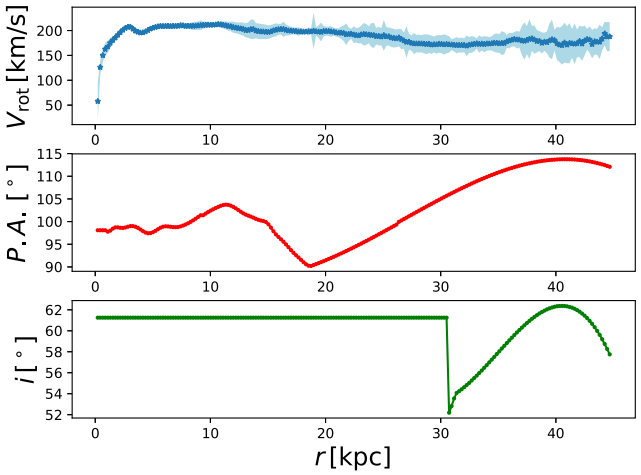

Figure 3. Final RC of NGC 5055 with uncertainties, derived using h_3 velocity field (top panel blue); adopted profiles for PA (middle panel – red) and i (bottom panel – green).

of the approaching or receding side of the galaxy in question, we left other parameters involved in the fitting as free, including PA and i. Uncertainties are shown in Fig. 3, and are used in the fitting of the dynamical models presented below (Section 4).

We compared the inner parts of our derived RC with the one based on an Hα data with higher spatial resolution available from work of Blais-Ouellette et al. (2004), and we found an excellent agreement.

For DDO 154, the situation was much simpler when it comes to stability of PA and i. We used a similar prescription of first setting the centre, then systemic velocity, and then deriving the PA and i radial profiles. For the centre, we also found that it is satisfactory to fix it to the position found by Trachternach et al. (2008), see Table 2. Most of the values for $V_{\rm sys}$ were clustered around $V_{\rm sys} = (375.5 \pm 5.5)\,{\rm km\,s^{-1}}$, so this value was taken and fixed in the subsequent run of `rotcur`. Radial distributions of PA and i were cleaned out of 3σ outliers using an appropriate polynomial fit (that we do not use for the final distribution), and smoothed out by running mean smoothing with kernel width equal to three. Parameter values were fixed to these series of values in the last run of the `rotcur`, from which we derive the final RC. We show the adopted values for PA and i in Fig. 4, in the middle and bottom panels.

Conservative estimates on rotation velocity errors described above for NGC 5055 were also used in the case of DDO 154.

3 DYNAMICAL MODELLING

The RCs for galaxies NGC 5055 and DDO 154 that we derived and used in our dynamical models are shown in Figs 3 and 4, respectively.

In all calculations for NGC 5055 and DDO 154, we use the fixed distance of (8.99 ± 0.45) and (4.04 ± 0.20) Mpc, respectively,

Downloaded from https://academic.oup.com/mnras/article/469/3/3564/3779716 by Access provided by HEAL-Link (University of Athens) user on 12 December 2022

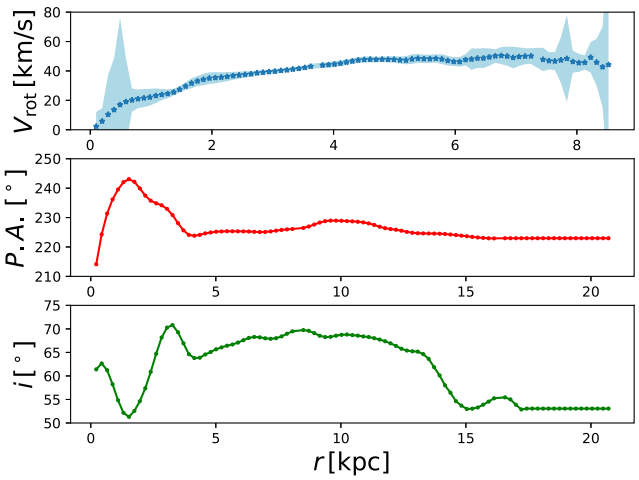

Figure 4. Final RC of DDO 154 with uncertainties, derived using h_3 velocity field (top panel – blue); adopted profiles for PA (middle panel – red), and i (bottom panel – green).

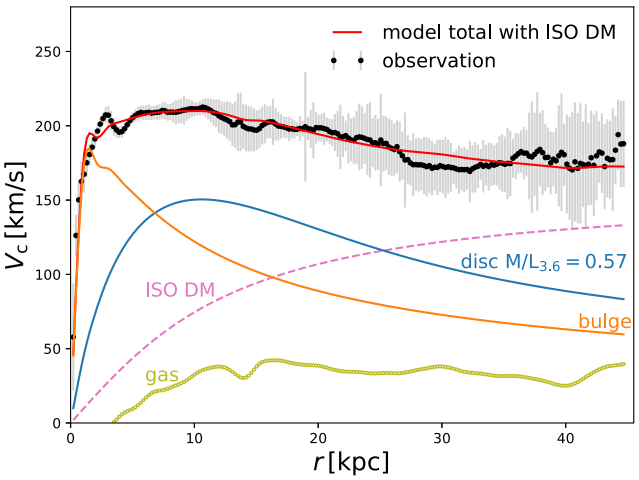

Figure 5. The best-fitting model of NGC 5055 for the ISO DM Newtonian model and the adopted distance of 8.99 Mpc. The *blue* line is the contribution of the disc, the *yellow* line is the contribution of the bulge, and the thick *green* line with open circles represents the contribution of the gas. The contribution of the ISO halo is plotted with the dashed *purple* line and the best-fitting model is shown with the *red* solid line. See the text for details.

from most up-to-date distance measurements from Extragalactic Distance Database[8] (EDD; Tully et al. 2009). Galactocentric radii in arcseconds were rescaled to kiloparsecs for the adopted galaxy distance. In the case of NGC 5055, the conversion is approximately 1 kpc ∼ 23 arcsec, and in the case of DDO 154, the scale is 1 kpc ∼ 51 arcsec.

3.1 Stellar and gas component

In all our models below, we take into account the baryonic contribution from the stellar component and the gas component:

$$V^2_{\rm rot,bar} = V^2_* + V^2_{\rm gas}. \quad (3)$$

Here, the stellar component is an exponential disc for DDO 154, and a disc and bulge for NGC 5055:

$$V^2_* = \begin{cases} V^2_{\rm bulge} + V^2_{\rm disc}, & \text{for NGC 5055,} \\ V^2_{\rm disc}, & \text{for DDO 154.} \end{cases} \quad (4)$$

Contribution to the total mass and therefore RCs of galaxies from model exponential discs and spherical bulge surface densities are calculated using GIPSY task `rotmod`. Calculation of rotational velocity for truncated exponential disc in `rotmod` relies on work of Casertano (1983). The van der Kruit & Searle (1981) law was assumed to take into account the finite thickness of the fitted exponential disc in z:

$$\Sigma \propto \frac{\mathrm{sech}^2\left(\frac{z}{z_0}\right)}{z_0}. \quad (5)$$

From the surface brightness of outer components, we obtained a reasonable estimate of the disc scalelengths, and from this, disc scaleheights were calculated as $0.2r_s$ (as in our previous work Samurović, Vudragović & Jovanović 2015), which gives approximate values of $z_0 = 0.917$ kpc for NGC 5055, and $z_0 = 0.100$ kpc for DDO 154 (values are listed in Table 1). The spherical bulge rotation velocity was based on model surface densities that are adopted from GALFIT fit, and described in Section 2.1 and Table 1. `rotmod` task was again used for the calculation.

[8] Available at: http://edd.ifa.hawaii.edu/

Similarly to the stellar disc and bulge, contribution to the total mass from gaseous disc is calculated using GIPSY task `rotmod`. From the observed distribution of surface brightness in H I, we could not obtain a reasonable estimate of the gas disc scalelength (and therefore height), so we used the approximate values. For NGC 5055 again, the van der Kruit & Searle (1981) sech^2 law is assumed with approximative disc scaleheight of 0.20 kpc (listed in Table 1), which is a satisfying approximation for the characteristic height of gaseous discs in massive spirals (for the same approximation see Samurović et al. 2015).

In the case of DDO 154, there are strong indications found by several authors that the gas disc has non-zero thickness in dwarf galaxies (Banerjee et al. 2011; Stilp et al. 2013). This thickness problem has been found in the FIGGS sample (Begum et al. 2008; Roychowdhury et al. 2010). We decided on the exponential disc approximation for the vertical component as well, with z_0 value found by Stilp et al. (2013) of 0.708 kpc (listed in Table 1). Stilp et al. (2013) derived the thickness of DDO 154's gas disc based on a method discussed by Ott et al. (2001). Value derived by Stilp et al. (2013) is comparable with one calculated by Angus et al. (2012) in MONDian framework. Contribution to the rotation velocity was again calculated with `rotmod` task for the double exponential gas disc with finite thickness.

The observed neutral gas rotational velocity in the case of NGC 5055 was smoothed before adding it to other components and fitting procedure, and is shown in that form (Figs 5 and 6).

3.2 Newtonian dynamical models with dark matter

For Newtonian models with DM, we generally write the rotation velocity as:

$$V^2_{\rm c}(r) = V^2_{\rm rot,bar} + V^2_{\rm DM}, \quad (6)$$

where DM in our case is going to stand for the two most popular DM models that we also use: ISO model (see e.g. Jimenez et al. 2003) and Navarro, Frenk & White cold dark matter model (NFW CDM, Navarro, Frenk & White 1997).

Downloaded from https://academic.oup.com/mnras/article/469/3/3564/3779716 by Access provided by HEAL-Link (University of Athens) user on 12 December 2022

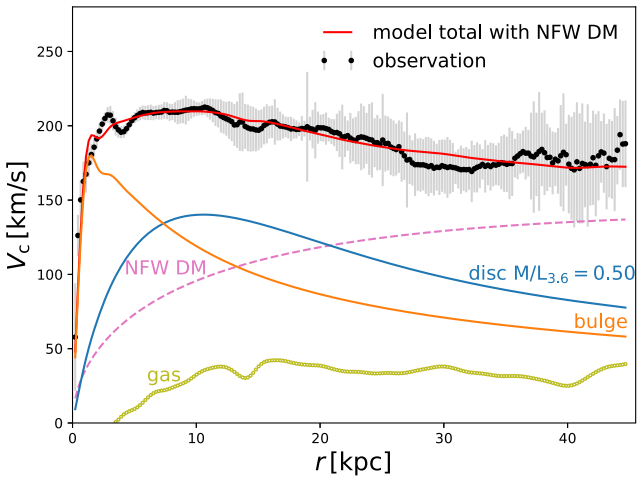

Figure 6. The best-fitting model of NGC 5055 for the NFW DM Newtonian model and the adopted distance of 8.99 Mpc. The *blue* line is the contribution of the disc, the *yellow* line is the contribution of the bulge, and the thick *green* line with open circles represents the contribution of the gas. The contribution of the NFW halo is plotted with the dashed *purple* line and the best-fitting model is shown with the *red* solid line. See the text for details.

3.2.1 *Isothermal sphere model*

For ISO model, we write the rotation velocity as:

$$V_c^2(r) = V_{\rm rot,bar}^2 + V_{\rm ISO}^2, \tag{7}$$

where $V_{\rm ISO}^2$ is the contribution from the dark halo.

We then write the density profile of the DM pseudo-ISO as (Jimenez et al. 2003):

$$\rho = \rho_0 \left[1 + \left(\frac{R}{R_c}\right)^2\right]^{-1}, \tag{8}$$

where ρ_0 represents the finite central density and R_c is the core radius. For this profile, it can be shown that the corresponding RC can be written in the following form:

$$V_{\rm ISO}^2 = 4\pi G \rho_0 R_c^2 \left[1 - \frac{R_c}{R} \arctan\left(\frac{R}{R_c}\right)\right]. \tag{9}$$

The dark halo is added to the baryonic component in ISO models, and the best-fitting models are presented in Section 4.1. ρ_0 and R_c are left as free parameters in the first set of models. In the second set, they are fixed following the developed procedure, which we explain in more detail in Section 3.3.1.

3.2.2 *NFW model*

For NFW model DM is added in the following form:

$$V_{\rm DM}^2(R) = V_{\rm CDM}^2(R) = G M_{\rm CDM}(R)/R, \tag{10}$$

and $M_{\rm CDM}(R)$ represents the mass of CDM enclosed within the radius R.

The use of high-resolution collisionless N-body simulations of structure formation within the framework of CDM cosmology led to the following form of the density profile (NFW):

$$\rho(R) = \rho_{\rm crit} \frac{\delta_0}{(R/R_s)(1 + R/R_s)^2}, \tag{11}$$

where $\rho_{\rm crit}$ is the critical density ($\rho_{\rm crit} = 277.3h^2$ M$_\odot$ kpc^{-3}, Navarro et al. 1997), δ_0 is a characteristic overdensity, and R_s is a scale radius (the distance at which the slope of the profile changes from -1 to -3). The logarithmic slope of the NFW profile at $R \sim R_s$ resembles an ISO (Mo, van den Bosch & White 2010). The concentration parameter, C, is defined as $C = R_{200}/R_s$, where $R_{200} = (M_{200}/(4\pi/3 \times 200\rho_{\rm crit}))^{1/3}$ and M_{200} is the virial mass. The DM mass within an enclosed radius R (expressed through $x \equiv R/R_s$) is:

$$M_{\rm CDM}(x) = 4\pi\rho_s R_s^3 \left[\ln(1+x) + \frac{x}{1+x}\right], \tag{12}$$

where ρ_s is the density at R_s. The NFW halo is added to the purely baryonic mass, obtained using the stellar and gas components.

In all of our NFW models, as in the case of the ISO approach, the best-fitting models are presented in Section 4.1, and similarly, C and R_{200} are free parameters in the fits.

3.3 The modelling procedure

For each of our dynamical models, the goodness-of-fit using χ^2 statistic has been calculated and values are listed in Table 3.

Best-fitting for different models and model parameters is found by minimizing the χ^2:

$$\chi^2 = \sum_{i=1}^{N} \left[\frac{p_i^{\rm obs} - p_i^{\rm mod}}{\Delta p_i^{\rm obs}}\right]^2, \tag{13}$$

where N is the number of data points, $p_i^{\rm obs}$ are the observed data points (Figs 3 and 4, top panels), the model values are given with $p_i^{\rm mod}$, and $\Delta p_i^{\rm obs}$ are the uncertainties of the observed values of the velocity at the given radius.

For the first set of models (Figs 5–7), we leave the $M/L_{3.6}$ parameter for the stellar component as a free parameter, in addition to the two free parameters that describe the DM model [(ρ_0, R_c) and (ρ_s, R_s), for ISO and NFW, respectively]. NFW model for DDO 154 is an exception (Fig. 10), where we had to fix $M/L_{3.6}$; otherwise the fitted parameters would be meaningless. M/L of the gas component was fixed to 1 in all cases (after the contribution of helium was accounted for with factor of 1.36, as stated above). We do, however, plan to address the issue of scaling between the observed neutral hydrogen to total gas content, neutral and molecular, in our future work, and how the more detailed treatment of gas affects dynamical modelling. $M/L_{3.6}$ value for disc, and bulge in the case of NGC 5055, was left free as stated above. From this kind of analysis, we obtained one overall value for $M/L_{3.6}$, describing globally given component of the galaxy in question at all radii. In Table 3, we give $\bar{\chi}^2$ values for best-fitting models for both galaxies and both DM models, together with M/L and corresponding masses of different components (see Table 4).

The second set of models explores how dynamical models work with constraints for $M/L_{3.6}$ coming from the SPS. We wanted to tackle the problem of deriving the radial profile of stellar disc's $M/L_{3.6}$, not by using the empirical relations between M/L and colour, but through the SPS modelling. SPS helped us derive reliable DM models for galaxies, and from that we constructed $M/L_{3.6}$ radial profiles for the stellar disc. The procedure we derived (which was used in the second set of the model fits) is described in more detail in Section 3.3.1.

3.3.1 *Stellar population synthesis models*

As in our previous work (Samurović et al. 2015), the SPS models that we use are from Bell & de Jong (2001) and Into

Downloaded from https://academic.oup.com/mnras/article/469/3/3564/3779716 by Access provided by HEAL-Link (University of Athens) user on 12 December 2022

Table 3. Best-fitting ISO and NFW dynamical models for NGC 5055 and DDO 154: Column (1): Galaxy ID. Column (2): The DM model. Column (3): Distance from EDD in megaparsecs. Column (4): The best-fitting bulge stellar M/L in the 3.6 μm band. Column (5): The best-fitting disc stellar M/L in the 3.6 μm band. Column (6): The R_c parameter of the ISO model in kiloparsecs. Column (7): The ρ_0 parameter of the ISO model in $10^{-3} M_\odot$ pc^{-3}. Column (8): The C parameter of the NFW model. Column (9): The R_{200} parameter of the NFW model in kiloparsecs. Column (10): The reduced $\tilde{\chi}^2$ value of the best-fitting model. '*' stands for maximum $M/L_{3.6}^{\rm disc}$ that is inside 1σ for the NFW model in the case of DDO 154 (see the text for details).

Galaxy ID	Model	D (Mpc)	$M/L_{3.6}^{\rm bulge}$	$M/L_{3.6}^{\rm disc}$	R_c (kpc)	ρ_0 ($10^{-3} M_\odot$ pc^{-3})	C	R_{200} (kpc)	$\tilde{\chi}^2$
(1)	(2)	(3)	(4)	(5)	(6)	(7)	(8)	(9)	(10)
NGC 5055	ISO	8.99	0.36 ± 0.01	0.57 ± 0.04	9.8 ± 2.7	4.8 ± 2.2	–	–	0.31
	NFW		0.35 ± 0.01	0.50 ± 0.05	–	–	2.8 ± 1.0	102 ± 7	0.31
DDO 154	ISO	4.04	–	0.25 ± 0.20	1.5 ± 0.1	26.2 ± 3.0	–	–	0.21
	NFW*		–	0.26	–	–	3.4 ± 0.2	40.3 ± 1.5	0.28

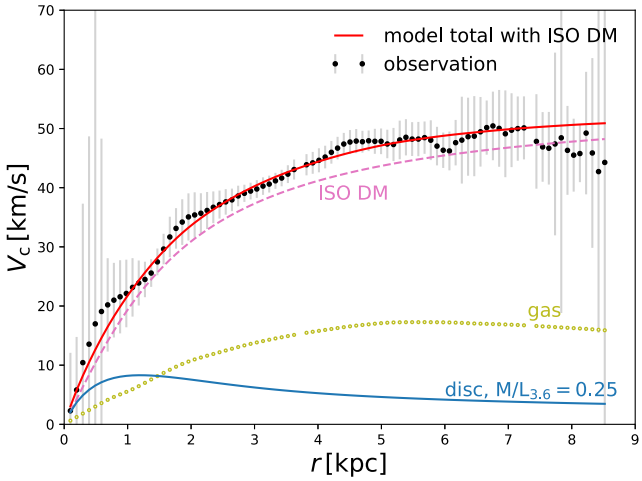

Figure 7. The best-fitting model of DDO 154 for the ISO DM Newtonian model and the adopted distance of 4.04 Mpc. The *blue* line is the contribution of the disc, and the thick *green* line with open circles represents the contribution of the gas. The contribution of the ISO halo is plotted with the dashed *purple* line and the best-fitting model is shown with the *red* solid line. See the text for details.

& Portinari (2013). SPS models use the colour of the galaxy and a rough estimate of its metallicity for the calculation of stellar M/L. We were able to determine a wide range of reliable colours based on measurements from Muñoz-Mateos et al. (2009) and Moustakas et al. (2010), as described below. Colours of galaxy DDO 154 were in all cases outside the ranges that could be described by the SPS models we used. DDO 154, as several studies find (Kennicutt & Skillman 2001; Komugi et al. 2011), is an extremely low-metallicity galaxy, and it does not have indicators as Mg_2 line-strength index measured, that we use in the case of a NGC 5055. Therefore, the subsequent analysis based on various SPS models was done only for NGC 5055.

In the case of NGC 5055, we used 13 different combinations of SPS models with initial mass functions (IMFs). From Bell & de Jong (2001), we used all available models, which include the Bruzual & Charlot (2003) model with Salpeter IMF (Salpeter 1955), scaled Salpeter and modified Salpeter IMF, the Bruzual & Charlot (1996) model with Scalo IMF (Scalo 1986), Kodama and Shultz models with Salpeter IMF, and the PEGASE[9] model, both with Salpeter IMF and its two modifications. These models are all based on single-age stellar populations (SSPs). More recent models of Into & Portinari (2013) use colour–M/L relations which include an accurate implementation of the thermally pulsating asymptotic giant branch phase and the effects of interstellar dust; they considered realistic chemical evolution models and the role of the mass–metallicity relation and metallicity gradients, which are important for the outskirts of disc galaxies. The estimates of the M/L (in 3.6 μm band) in Into & Portinari (2013) were derived for composite stellar populations (CSP, which stands for the convolution of simple stellar populations of different age and metallicity, according to a given star formation and chemical evolution). Models in Into & Portinari (2013) are based on the exponential SFH model with the Kroupa IMF (Kroupa 2001), and disc galaxy models are based on both Kroupa and Salpeter IMFs. The interstellar dust attenuation spiral galaxy model from Into & Portinari (2013) was also included.

For $B-V$ colour, all 13 models from both Bell & de Jong (2001) and Into & Portinari (2013) models are calculated, so SSP as well as CSP were used. Six other colours, spanning a wide range of wavelengths, from visible to IR, were used. They include five Sloan Digital Sky Survey (SDSS) colours: $g-r$, $g-i$, $g-z$, $r-i$ and $r-z$, and $B-K_S$ colour. SDSS magnitudes were taken from Muñoz-Mateos et al. (2009), and appropriate colours were calculated by us. $B-V$ colour was determined by Moustakas et al. (2010) and $B-K_S$ colour was calculated combining data from the two aforementioned papers, Muñoz-Mateos et al. (2009) and Moustakas et al. (2010). For these six colours (five SDSS colours and $B-K_S$), only models from Into & Portinari (2013) are available, so all the models are CSP, and based on Kroupa and Salpeter IMFs. All colours were corrected for foreground extinction beforehand (Schlegel, Finkbeiner & Davis 1998), and K-correction was determined to be not significant. For $B-V$ and $B-K_S$ colours, AB magnitudes were transformed to Vega system using Blanton & Roweis (2007).

For metallicity in the case of NGC 5055. we used a value of Mg_2 index from HyperLeda ($Mg_2 = 0.2$). From the work of Casuso et al. (1996), who used Mg_2 index as an indicator of metallicity, we conclude that $Z = 0.02\,Z_\odot$ is a satisfying approximation for metallicity. We use this value in our estimates.

Given that relations between $M/L_{3.6}$ and colour for a given metallicity range were not available, a conversion was needed. 3.6 μm band is closest to $K_S^{\rm 2MASS}$ band and Johnson K band, so we consider that this conversion introduces minimal error. Conversion factors from to 3.6 μm band to two K bands were calculated from Dale et al. (2007) from the available fluxes for each galaxy. Transformation between the two K bands was also needed, and considering that it may be derived only indirectly since Johnson standard stars are saturated in the 2MASS survey, an indirect relation from Carpenter (2001) was used.

31 $M/L_{3.6}$ values coming from different SPS models, as described above, were used to choose our most probable DM model. For every

[9] http://www2.iap.fr/users/fioc/PEGASE.html

Downloaded from https://academic.oup.com/mnras/article/469/3/3564/3779716 by Access provided by HEAL-Link (University of Athens) user on 12 December 2022

fixed value of $M/L_{3.6}$, we ran fitting of the data to find the best-fitting DM model. From DM model parameters, we constructed weighted histograms describing frequency for DM parameters of interest (see Figs 13 and 15). Weighing was done with goodness-of-fit reduced χ^2 value. Because R_c, in the case of ISO model, and R_{200}, in the case of NFW model, both showed strong preferences, respective parameter values (indicated in red in Fig. 12) were fixed and used to determine the other corresponding DM parameter (ρ_0 or C) by fitting procedure once again. The 'best' DM models were fixed in this way, and by additionally fixing contributions from the bulge and gas, we were able to derive stellar disc M/L profiles (Figs 14 and 16).

4 RESULTS

Here, we present results for dynamical modelling using DM models based on a pseudo-ISO and NFW models. As described, the stellar M/L for the bulge and the disc are free parameters in the first set of models. We compared the inferred M/L with the values coming from the SPS models that we use. The best-fitting results are presented in Figs 5–10 and in Table 3.

Using SPS values for M/L, we were able to derive their radial profiles, which are presented in Figs 14 and16.

In all our models, we estimate the M/L in the 3.6 μm band because we use the *Spitzer* S4G image of NGC 5055 and DDO 154 for the decomposition and derivation of the necessary structural parameters.

4.1 Dynamical models with free stellar mass-to-light ratio

The free parameters in the case of the ISO models were R_c and ρ_0, as described above.

The best-fitting ISO model for galaxy NGC 5055 (shown in Fig. 5) is of good quality ($\bar{\chi}^2 = 0.31$). The best-fitting stellar M/L for the bulge and the disc are $M/L_{3.6}^{\rm bulge} = (0.36 \pm 0.01)$ and $M/L_{3.6}^{\rm disc} = (0.57 \pm 0.04)$, respectively. The fitted DM parameters are $R_c = (9.8 \pm 2.7)$ kpc and $\rho_0 = (4.8 \pm 2.2)10^{-3}\, M_\odot\, {\rm pc}^{-3}$. Here, the values of the uncertainties that are obtained with `rotmas` are overestimated, but are still presented in this form in Table 3.

The dark halo in the NFW model, as described above, has two free parameters, C and R_{200}. The best fit ($\bar{\chi}^2 = 0.31$) for NFW model in the case of NGC 5055 was obtained for $M/L_{3.6}^{\rm bulge} = (0.35 \pm 0.01)$ and $M/L_{3.6}^{\rm disc} = (0.50 \pm 0.05)$, as values of the stellar M/L for the bulge and the disc, respectively. The values of CDM parameters are $C = (2.8 \pm 1.0)$ and $R_{200} = (102 \pm 7)$ kpc. We list them in Table 3 and show them in Fig. 6, along with all best-fitting free parameters. As in the case of the ISO model, the values of the uncertainties that are obtained are left in this form in Table 3.

The best-fitting ISO model for DDO 154 (shown in Fig. 7) yielded $M/L_{3.6}^{\rm disc} = (0.25 \pm 0.20)$, with R_c and ρ_0 as free parameters. It is of very good quality ($\bar{\chi}^2 = 0.16$). The best-fitting DM parameters are $R_c = (1.5 \pm 0.1)$ kpc and $\rho_0 = (26.2 \pm 3.0) \times 10^{-3}\, M_\odot\, {\rm pc}^{-3}$.

For the dark NFW model halo of DDO 154, we find the best-fitting value of $M/L_{3.6}^{\rm disc}$ is non-physical (i.e. negative). In this case, it seems that the lower the contribution from the stellar disc component, the better the fit is (consistent with previous findings, that list DDO 154 as a 'dark' galaxy, see e.g. Carignan & Freeman 1988; Kennicutt & Skillman 2001). Instead, we explored the parameter space of all three free parameters $M/L_{3.6}^{\rm disc}$, C and R_{200}, to try to find physically significant but still good models in terms of $\bar{\chi}^2$. In Figs 8 and 9, we show the contours of confidence levels (CLs) that are corresponding to models that are within 1σ–5σ regarding the value of $\bar{\chi}^2$, as an indicator of a quality of a fit. The CLs are plotted in $M/L_{3.6}^{\rm disc} - C$ and $M/L_{3.6}^{\rm disc} - R_{200}$ parameter spaces. We can see that all the models within 1σ from the best-fitting solution have negative $M/L_{3.6}^{\rm disc}$. From all the possible models that have $M/L_{3.6}^{\rm disc} > 0$, and are still of reasonable well quality (inside 3σ), we choose the model with larger disc mass, that is assessed to be $M/L_{3.6}^{\rm disc} = 0.26$. $M/L_{3.6}^{\rm disc}$ is, only in this case, a fixed parameter in the fitting procedure (Fig. 10). This best-fitting model had $\bar{\chi}^2 = 0.28$, and yielded values of CDM parameters $C = 3.4 \pm 0.2$ and $R_{200} = 40.3 \pm 1.5$, which are given in Table 3 (also shown in Figs 8 and 9 in red). The fixed value of $M/L_{3.6}^{\rm disc}$ is chosen with respect to the corresponding DM parameters. Ranges for DM parameters of all the possible physically meaningful models were $3.0 < C < 4.5$ and $35 < R_{200} < 45$. We chose the value of $M/L_{3.6}^{\rm disc}$ whose corresponding DM parameters were around the approximate centre of this range, and at the same time the $M/L_{3.6}^{\rm disc}$ was on the larger side (ranging from 0 to 0.3).

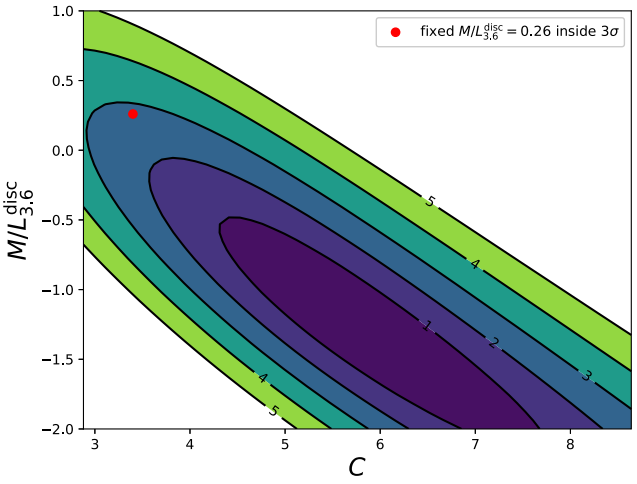

Figure 8. DDO 154 dynamical models with NFW halo: CL contours ranging from 1σ to 5σ are shown in CDM parameter $C - M/L_{3.6}^{\rm disc}$ parameter space. The chosen model with fixed $M/L_{3.6}^{\rm disc} = 0.26$ is shown in red.

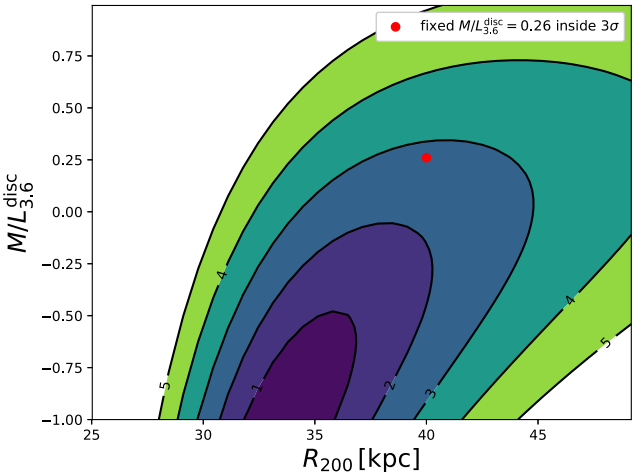

Figure 9. DDO 154 dynamical models with NFW halo: CL contours ranging from 1σ to 5σ are shown in CDM parameter $R_{200} - M/L_{3.6}^{\rm disc}$ parameter space. The chosen model with fixed $M/L_{3.6}^{\rm disc} = 0.26$ is shown in red.

Downloaded from https://academic.oup.com/mnras/article/469/3/3564/3779716 by Access provided by HEAL-Link (University of Athens) user on 12 December 2022

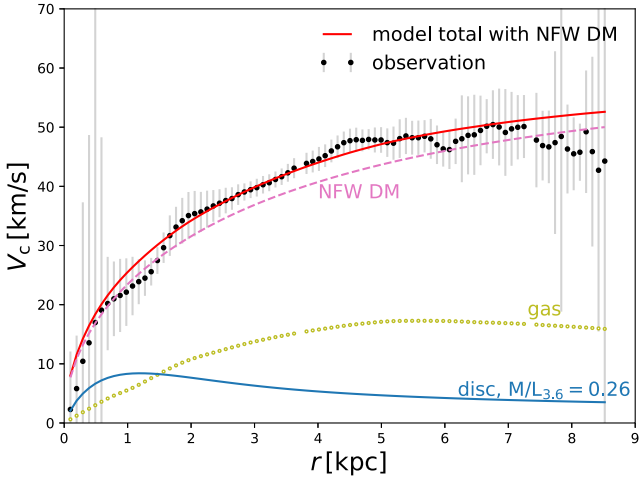

Figure 10. The adopted model of DDO 154 for the NFW DM Newtonian model and the adopted distance of 4.04 Mpc and the value of $M/L_{3.6}^{\rm disc}$ fixed to 0.26. The *blue* line is the contribution of the disc, and the thick *green* line with open circles represents the contribution of the gas. The contribution of the NFW halo is plotted with the dashed *purple* line and the best-fitting model is shown with the *red* solid line. See the text for details.

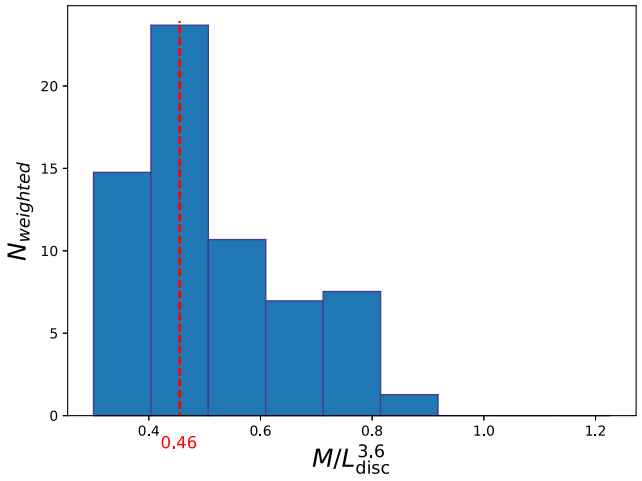

Figure 11. $\bar{\chi}^2$-weighted histogram constructed for SPS $M/L_{3.6}^{\rm disc}$ values in the case of NGC 5055.

4.2 Constraints on $M/L_{3.6}^{\rm disc}$ from SPS models in the case of NGC 5055

As described in Section 3.3.1, we used SPS models available in Bell & de Jong (2001) and Into & Portinari (2013), based on different IMFs. The weighted histogram of $M/L_{3.6}^{\rm disc}$ values (Fig. 11) is the result of usage of SPS models with seven different colours, and it gives the 'best' (3σ-clipped median) value of (0.46 ± 0.05) for the $M/L_{3.6}^{\rm disc}$. The weighing is done with the goodness-of-fit indicator, $\bar{\chi}^2$.

Value of $M/L_{3.6}^{\rm disc}$ from NFW model is consistent within uncertainty with the most probable value of $M/L_{3.6}$ from our SPS models (shown in Fig. 11), while the best-fitting value from ISO model falls slightly outside that range (shown bellow, in Fig. 12). In order to find the most probable, or 'best' DM model we re-run the fitting of the observed RC in `rotmas`, but this time with fixed SPS $M/L_{3.6}^{\rm disc}$ values. All 31 single values of $M/L_{3.6}^{\rm disc}$ calculated from SPS models were used (see Sections 3.3.1 and 4.3 for details).

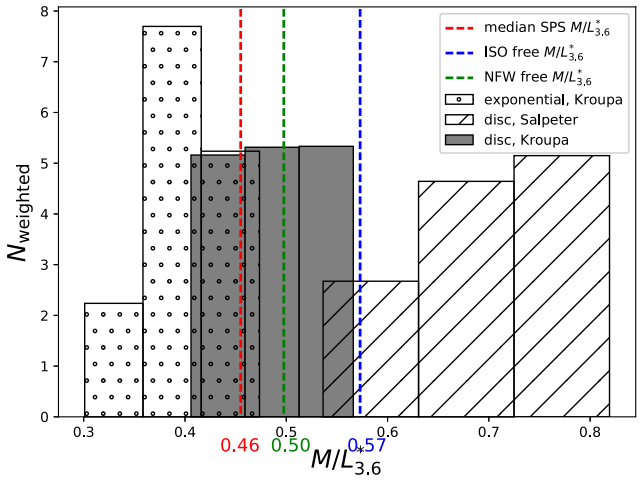

Figure 12. Three of the SPS models for NGC 5055 that yielded 68 per cent of the generated $M/L_{3.6}^{*}$ values, all based on Into & Portinari (2013): exponential model based on Kroupa IMF, disc model based on Kroupa IMF, and disc model based on Salpeter IMF.

The best-fitting model and other models inside the 1σ region are closer to the DM parameters with $M/L_{3.6}^{\rm disc}$ values inferred for Kroupa IMF. Because three of the CSP models calculated by Into & Portinari (2013) are used with all the seven listed colours, we show their $M/L_{3.6}^{\rm disc}$ distribution in Fig. 12. The disc model from Into & Portinari (2013), based on Kroupa IMF, shows particularly good agreement with the best-fitting $M/L_{3.6}^{\rm disc}$ value for NFW model, and is generally closest to the best overall SPS value inferred from the weighted histogram. Over all used colours this model shows less variance than the others, and it is consistent with best-fitting $M/L_{3.6}^{\rm disc}$ within uncertainties for most colours (Fig. 12).

4.3 Radial profiles of $M/L_{3.6}^{\rm disc}$ for NGC 5055

All the values of $M/L_{3.6}^{\rm disc}$ that were the output of the SPS models (31 of them), were kept as a fixed parameter in the re-run of the fitting of the RC. This was done as an attempt to derive the most probable DM model, both with ISO and NFW parameters.

In the case of ISO models, we have a clear preference in the case of $R_{\rm c}$. The most probable value for $R_{\rm c}$ was found to be $R_{\rm c} = (7.6 \pm 5.2)$ kpc (weighted histogram shown in Fig. 13). For the observed RC, the observed contribution of the gas, the ISO model of DM with parameters fixed to $(R_{\rm c}, \rho_0) = (7.6, 7.5)$, and the rotational velocity from the mass enclosed in a bulge with $M/L_{3.6}^{\rm bulge} = 0.37$ (value from best-fitting solution), we derived the radial profile of $M/L_{3.6}^{\rm disc}$ using:

$$M/L_{3.6}^{\rm disc} = \frac{V_{\rm disc,calc}^2}{V_{\rm disc,obs}^2}, \tag{14}$$

where:

$$V_{\rm disc,calc}^2 = V_{\rm c}^2 - V_{\rm bulge}^2 - V_{\rm gas}^2 - V_{\rm DM}^2, \tag{15}$$

and $V_{\rm disc,obs}^2$ is the rotational velocity due to mass contained in the stellar disc calculated from surface brightness profile with no scaling (M/L equal to 1). Radial profile of $M/L_{3.6}^{\rm disc}$ derived in the described manner is shown in Fig. 14), along with the linear fit to the 3σ-clipped set of radial $M/L_{3.6}^{\rm disc}$ values. We found the justification for the described procedure in the fact that most of the uncertainty of the baryonic component comes from the M/L of a stellar disc, so

Downloaded from https://academic.oup.com/mnras/article/469/3/3564/3779716 by Access provided by HEAL-Link (University of Athens) user on 12 December 2022

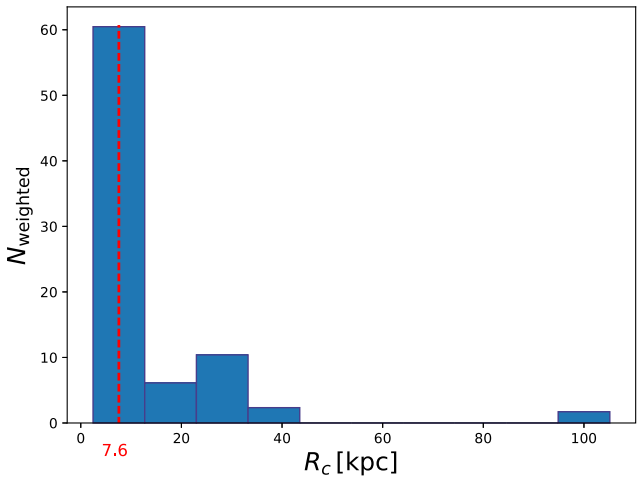

Figure 13. $\bar{\chi}^2$-weighted histogram of the ISO parameter R_c, constructed for SPS-fixed $M/L_{3.6}^{disc}$ values in the case of NGC 5055.

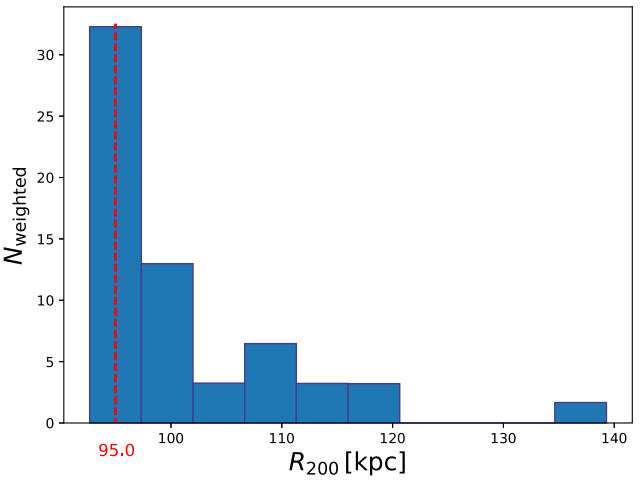

Figure 15. $\bar{\chi}^2$-weighted histogram of the NFW parameter R_{200}, constructed for SPS-fixed $M/L_{3.6}^{disc}$ values in the case of NGC 5055.

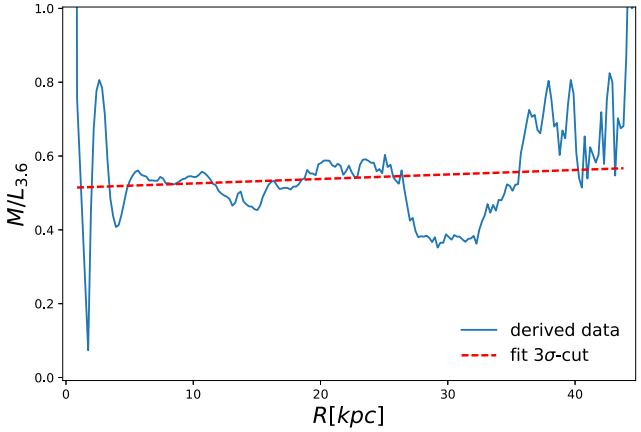

Figure 14. Radial profile of $M/L_{3.6}^{disc}$ for NGC 5055 in ISO model: raw data (blue line) and 3σ-clipped fit (red dashed line).

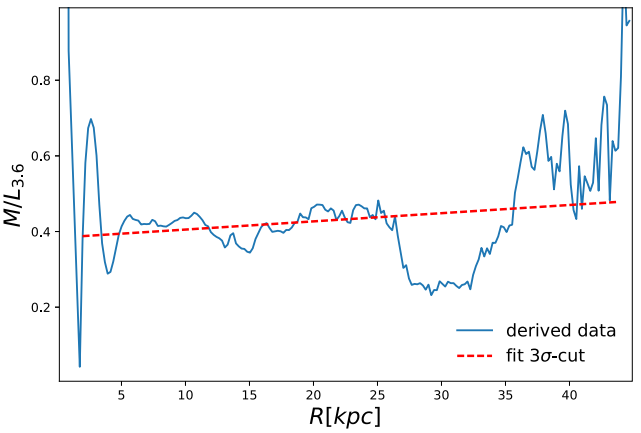

Figure 16. Radial profile of $M/L_{3.6}^{disc}$ for NGC 5055 in NFW model: raw data (blue line) and 3σ-clipped fit (red dashed line).

M/L of other components can be taken as one constant value at all radii for this approximation.

For NFW models, the parameter R_{200} shows a preferred value. The most probable value from the weighted histogram of R_{200} is found to be $R_{200} = (95.0 \pm 2.3)$ kpc (Fig. 15). We explored in more detail the behaviour of the $\bar{\chi}^2 = f(R_{200})$ and found that minimum of the function corresponds to the best-histogram value within uncertainties. For the NFW DM model, parameters were fixed to (C, R_{200}) = (4.8, 95.0). M/L of the bulge was fixed to the best-fitting solution with the above CDM parameters, which is $M/L_{3.6}^{bulge} = 0.34$. From the observed RC, the observed contribution of the gas, rotational velocity due to mass of the bulge, and the DM component we derived the radial profile of $M/L_{3.6}^{disc}$ using equations (14) and (15). The radial profile of $M/L_{3.6}^{disc}$ derived in the described manner is shown in Fig. 16, along with the linear fit to the 3σ-clipped set of radial $M/L_{3.6}^{disc}$ values, same as for the ISO model.

The dips (lower values of $M/L_{3.6}^{disc}$ from 26 to 34 kpc) that are present in radial profiles are the artefacts of the dip in the corresponding RC, which we believe is a consequence of the reduction procedure, and not real. At the same time, we did not want to introduce any post-processing to the tilted-ring fitting procedure and derivation of the RC, so we left it in its original form. We suspect that the incorrect value of i parameter is responsible for the fall in the value of rotational velocity. Also, there are less observation points in these rings, and fits are less reliable.

5 DISCUSSION

We now look at the results from the mass models and the treatment of the stellar $M/L_{3.6}$ in a broader context. For the two galaxies in question, we calculated the masses of individual components for various mass models (Table 4). These two galaxies follow general trends in terms of their RC shapes and their change with the luminosity and mass (de Blok et al. 2008, and the references therein). Luminous galaxies show sharp rise of rotational velocity with increased radius and flat behaviour in the outer regions. In contrast, low luminosity galaxies show a slower, steadier increase in rotational velocity over all of the observed disc. The masses of galactic components and mass fractions are given up to the last observed radii (the same ones that we show in our mass models). The actual masses of the galaxies are much larger if we take into account the DM masses of their whole haloes. The mass contribution of the DM component for a presumed theoretical profile (which might not be true) can be calculated without any additional assumptions. The mass of the stellar component, which is the large source of uncertainty and a subject of this paper, can only be assessed up to the

Downloaded from https://academic.oup.com/mnras/article/469/3/3564/3779716 by Access provided by HEAL-Link (University of Athens) user on 12 December 2022

Table 4. Masses of the galaxy components and baryonic fraction for the various used models with ISO or NFW DM component and applied to the two tested galaxies, NGC 5055 and DDO 154: $M_{\rm disc}$ – mass of the modelled disc component; $M_{\rm bulge}$ – mass of the modelled bulge component (in the case of NGC 5055); $M_{\rm gas}$ – mass of the neutral gas component; $M_{\rm total}$ – mass of the model for all components combined $M_{\rm baryon} + M_{\rm DM}$; $\frac{M_{\rm baryon}}{M_{\rm total}}$ – baryonic fraction up to the last observed radius ($\frac{M_{\rm baryon}}{M_{\rm total}}$ and $\frac{M_{\rm baryon}}{M_{\rm halo}}$ – ratio between the two main components of the total modelled galaxy mass up to the last observed radius. '*' – contribution from the gas component was fixed to 1 and thus given without uncertainties.

Galaxy ID	Model	$M_{\rm disc}$ $(10^8 M_\odot)$	$M_{\rm bulge}$ $(10^8 M_\odot)$	$M^*_{\rm gas}$ $(10^8 M_\odot)$	$M_{\rm total}$ $(10^8 M_\odot)$	$\frac{M_{\rm baryon}}{M_{\rm total}}$	$\frac{M_{\rm baryon}}{M_{\rm halo}}$
NGC 5055	Best-fitting ISO	796 ± 60	369 ± 7	163	3200 ± 1700	0.42 ± 0.25	0.72 ± 0.69
	Best-fitting NFW	691 ± 66	351 ± 5		3150 ± 510	0.38 ± 0.09	0.62 ± 0.18
DDO 154	Best-fitting ISO	0.27 ± 0.21	–	5.0	51 ± 12	0.10 ± 0.03	0.11 ± 0.04
	Best-fixed NFW	0.28	–		55 ± 5	0.10 ± 0.01	0.11 ± 0.01
NGC 5055	Radial profile $M/L^{\rm disc}_{3.6}$ ISO	752 ± 12	375 ± 0	163	3148 ± 59	0.41 ± 0.12	0.70 ± 0.03
	Radial profile $M/L^{\rm disc}_{3.6}$ NFW	606 ± 13	344 ± 5		3069 ± 88	0.36 ± 0.02	0.57 ± 0.03

last observing point. The baryonic mass fraction of the total and halo mass are thus much larger when given in their usual form (here we only inspect the parts where conventional matter is dominant). This representation is however satisfying for contrasting the two inspected galaxies and their mass models. We do note that the baryons from a halo, that are likely to be in a state of a coronal gas, should contribute to the overall inferred baryonic mass (and baryonic fraction). For NGC 891, a galaxy with a similar rotation velocity, a hot halo has been found (cf. Hodges-Kluck & Bregman 2013), with baryonic mass few times $10^8 M_\odot$. For our Galaxy, Tepper-García, Bland-Hawthorn & Sutherland (2015) (see also Bland-Hawthorn & Gerhard 2016) argue for a hot gas model with a few times $10^{10} M_\odot$, which is more than the neutral gas mass. Although not negligible, the assessments for the mass of the hot halo gas are still smaller than the uncertainty that we have in the baryonic mass and especially total mass, so we can say that our results are pointing out to a small baryonic fraction and are in concordance with the previously established missing baryon problem.

Models show that baryons in the halo are likely to be in the state of coronal gas at temperatures close to the virial temperature for specific total galaxy mass, with a fraction cooling into photoionized phase at $\sim 10^4$ K, potentially detectable in emission (e.g. Ćirković, Bland-Hawthorn & Samurović 1999). High-sensitivity extreme UV and X-ray observations and other methods are necessary in order to account for those halo baryons (Yoon & Putman 2013).

In the case of NGC 5055, both DM models give a similar value for the mass of a stellar disc and total mass. The ISO model gives a larger value for the mass of the stellar disc (for about 15 per cent) and the total mass (for about 2 per cent). The derived $M/L^{\rm disc}_{3.6}$ profile gives a smaller value of the mass for both tested DM models (about 5 per cent and 12 per cent, for ISO and NFW models respectively). However, the difference in mass when using the ISO model or the radial profile is still small compared to the total derived mass and cannot account for the missing baryons problem.

As expected, DDO 154 has a very small value for the baryon fraction of total mass, around four times smaller than the spiral galaxy. Both chosen ISO and NFW models give similar values for the mass of the stellar disc, and NFW model gives a larger value for the total mass (for about 3 per cent). Gas is a more dominant component in terms of mass for this galaxy, which also makes this case a peculiar one. With more significant gas mass and a grossly dominant DM mass, the two fitted DM models give the same baryonic fraction.

6 CONCLUSIONS

We analysed Newtonian models of the spiral galaxy NGC 5055 and dwarf irregular galaxy DDO 154 using several publicly available data bases. We used THINGS H I observations to determine the RCs and gas contributions, and S4G photometric observations in the 3.6 μm band to decompose the surface brightness profiles of the galaxies. Publicly available software packages such as GIPSY, IRAF, and GALFIT were used to extract the observational parameters needed for the dynamical modelling. The inferred *M*/*L* were compared with the estimates from the SPS models. In all our models, the gas contribution was taken as measured and not scaled to account for any other gas contributions to the mass. Distances were taken from the EDD and kept fixed in all our models. The conclusions are as follows:

(i) Both DM models for both galaxies were able to fit the observed RCs. Both the ISO and NFW models were able to fit the RC of NGC 5055 with the same quality of fit, $\bar{\chi}^2 = 0.31$. In the case of DDO 154, the ISO model was of an even better quality with $\bar{\chi}^2 = 0.16$. The NFW model used in fitting the RC of DDO 154 was unable to converge to a single physically sensible value but there were a number of possible models which were of good quality. We chose one of the good models with a fixed maximum value of $M/L^{\rm disc}_{3.6}$, and we obtained the goodness-of-fit of $\bar{\chi}^2 = 0.28$.

(ii) For NGC 5055, the inferred *M*/*L* of the stellar components were $M/L^{\rm disc}_{3.6} = 0.57$ and 0.36 for the ISO model, and $M/L^{\rm disc}_{3.6} = 0.50$ and 0.35 for the NFW model. Only the $M/L^{\rm disc}_{3.6}$ for NFW models was consistent within uncertainties with the 'best' SPS value of $M/L^{\rm SPS}_{3.6} = 0.46 \pm 0.05$. For DDO 154, we obtained $M/L^{\rm disc}_{3.6} = 0.25$ for the ISO model, and we fixed the $M/L^{\rm disc}_{3.6}$ to 0.26 for the NFW model. In this instance, the $M/L^{\rm disc}_{3.6}$ value was chosen as the optimal value (positive and inside 3σ). $M/L_{3.6}$ values from our models describing NGC 5055 were in line with the prediction from Meidt et al. (2014) to be satisfyingly described with a single value of 0.6 and to have smaller variations overall, and models for DDO 154 were not. The estimate of an *M*/*L* from the SPS models was not possible for DDO 154.

(iii) For NGC 5055, it was possible to calculate the SPS *M*/*L* for seven different colours, and we conclude that the disc model from Into & Portinari (2013) based on Kroupa IMF provides the value of $M/L_{3.6}$ that is closest to the best-fitting values and is most consistent internally. Further improvement in our understanding of the IMF would be of great significance for our work.

Downloaded from https://academic.oup.com/mnras/article/469/3/3564/3779716 by Access provided by HEAL-Link (University of Athens) user on 12 December 2022

(iv) Based on the SPS models of NGC 5055, we were able to derive the 'best' DM model, for both the ISO and NFW. From the chosen DM models, we derive the radial profile of the $M/L_{3.6}^{\rm disc}$. This method provides a profile that is independent from correlations with colour and thus can be used for comparison.

(v) We conclude that the used DM model does not affect the inferred fractions of the baryonic mass of these two very different galaxies, as long as it can provide a fit of satisfying quality to the observed RC. This is highly encouraging from the point of view of constructing a truly universal BMF of galaxies, dependent only on morphological parameters and the epoch of cosmic time. This will, in synergy with the Lyα absorption studies, microlensing, integral field spectroscopy studies and other relevant observational methods, enable us to precisely track the entire history of baryons in the universe, from the epoch of nucleosynthesis to the present day.

ACKNOWLEDGEMENTS

We acknowledge the support from the Ministry of Education, Science and Technological Development of the Republic of Serbia through project no. 176021 'Visible and Invisible Matter in Nearby Galaxies: Theory and Observations'. This research made use of the NASA/IPAC Extragalactic Database (NED), which is operated by the Jet Propulsion Laboratory, California Institute of Technology, under contract with the National Aeronautics and Space Administration. We acknowledge the usage of the HyperLeda data base (http://leda.univ-lyon1.fr). This work made use of THINGS, 'The H I Nearby Galaxy Survey.' We gratefully acknowledge the valuable comments of the referee Prof. A. Bosma, which helped to improve the quality of the manuscript. We thank Dr. W. J. G. de Blok for providing us valuable information about the work he performed with the THINGS team. We thank Dr. S. McGaugh for his advice regarding some observational aspects of spiral galaxies. We thank Dr. L. Portinari for clarification of her work. We thank Dr. Pavel Kroupa, Dr. Michal Bilek, Dr. Ana Vudragović and Milan Stojanović for the interesting discussions on the subject. We thank Dane Rukavina on his support. Most of all, we thank Dr. Srdjan Samurović and Dr. Milan M. Ćirković for being patient mentors, colleagues and friends, all of which made this work possible.

REFERENCES

Angus G. W., van der Heyden K. J., Famaey B., Gentile G., McGaugh S. S., de Blok W. J. G., 2012, MNRAS, 421, 2598
Banerjee A., Jog C. J., Brinks E., Bagetakos I., 2011, MNRAS, 415, 687
Battaglia G., Fraternali F., Oosterloo T., Sancisi R., 2006, A&A, 447, 49
Baugh C. M., 2006, Rep. Prog. Phys., 69, 3101
Begeman K. G., 1987, PhD thesis, Kapteyn Institute
Begum A., Chengalur J. N., Karachentsev I. D., Sharina M. E., Kaisin S. S., 2008, MNRAS, 386, 1667
Bell E. F., de Jong R. S., 2001, ApJ, 550, 212
Bell E. F., McIntosh D. H., Katz N., Weinberg M. D., 2003, ApJ, 585, L117
Blais-Ouellette S., Amram P., Carignan C., Swaters R., 2004, A&A, 420, 147
Bland-Hawthorn J., Gerhard O., 2016, ARA&A, 54, 529
Blanton M. R., Roweis S., 2007, AJ, 133, 734
Carignan C., Freeman K. C., 1988, ApJ, 332, L33
Carpenter J. M., 2001, AJ, 121, 2851
Casertano S., 1983, MNRAS, 203, 735
Casuso E., Vazdekis A., Peletier R. F., Beckman J. E., 1996, ApJ, 458, 533
Churchill C. W., Vander Vliet J. R., Trujillo-Gomez S., Kacprzak G. G., Klypin A., 2015, ApJ, 802, 10
Ćirković M. M., Bland-Hawthorn J., Samurović S., 1999, MNRAS, 306, L15
Dale D. A. et al., 2007, ApJ, 655, 863
de Blok W. J. G., Walter F., Brinks E., Trachternach C., Oh S.-H., Kennicutt R. C., Jr, 2008, AJ, 136, 2648
Draine B. T., Lee H. M., 1984, ApJ, 285, 89
Fukugita M., Hogan C. J., Peebles P. J. E., 1998, ApJ, 503, 518
Hodges-Kluck E. J., Bregman J. N., 2013, ApJ, 762, 12
Into T., Portinari L., 2013, MNRAS, 430, 2715
Jimenez R., Verde L., Treu T., Stern D., 2003, ApJ, 593, 622
Kennicutt R. C., Jr, Skillman E. D., 2001, AJ, 121, 1461
Komugi S., Yasui C., Kobayashi N., Hatsukade B., Kohno K., Sofue Y., Kyu S., 2011, PASJ, 63, L1
Kroupa P., 2001, MNRAS, 322, 231
Lanzetta K. M., Bowen D. V., Tytler D., Webb J. K., 1995, ApJ, 442, 538
Leroy A. K., Walter F., Brinks E., Bigiel F., de Blok W. J. G., Madore B., Thornley M. D., 2008, AJ, 136, 2782
Meidt S. E. et al., 2014, ApJ, 788, 144
Miller M. J., Hodges-Kluck E. J., Bregman J. N., 2016, ApJ, 818, 112
Mo H., van den Bosch F. C., White S., 2010, Galaxy Formation and Evolution. Cambridge Univ. Press, Cambridge, UK
Moustakas J., Kennicutt R. C., Jr, Tremonti C. A., Dale D. A., Smith J.-D. T., Calzetti D., 2010, ApJS, 190, 233
Muñoz-Mateos J. C. et al., 2009, ApJ, 703, 1569
Muñoz-Mateos J. C. et al., 2015, ApJS, 219, 3
Navarro J. F., Frenk C. S., White S. D. M., 1997, ApJ, 490, 493
Oh S.-H., de Blok W. J. G., Brinks E., Walter F., Kennicutt R. C., Jr, 2011, AJ, 141, 193
Ott J., Walter F., Brinks E., Van Dyk S. D., Dirsch B., Klein U., 2001, AJ, 122, 3070
Pahre M. A., Ashby M. L. N., Fazio G. G., Willner S. P., 2004, ApJS, 154, 235
Papastergis E., 2013, PhD thesis, Cornell Univ.
Papastergis E., Cattaneo A., Huang S., Giovanelli R., Haynes M. P., 2012, ApJ, 759, 138
Peng C. Y., Ho L. C., Impey C. D., Rix H.-W., 2010, AJ, 139, 2097
Querejeta M. et al., 2015, ApJS, 219, 5
Read J. I., Trentham N., 2005, Phil. Trans. R. Soc. Lond. Ser. A, 363, 2693
Rees M. J., Ostriker J. P., 1977, MNRAS, 179, 541
Roychowdhury S., Chengalur J. N., Begum A., Karachentsev I. D., 2010, MNRAS, 404, L60
Salo H. et al., 2015, ApJS, 219, 4
Salpeter E. E., 1955, ApJ, 121, 161
Salucci P., Persic M., 1999, MNRAS, 309, 923
Samurović S., Vudragović A., Jovanović M., 2015, MNRAS, 451, 4073
Scalo J. M., 1986, Fund. Cosmic Phys., 11, 1
Schlegel D. J., Finkbeiner D. P., Davis M., 1998, ApJ, 500, 525
Sheth K. et al., 2010, PASP, 122, 1397
Stilp A. M., Dalcanton J. J., Warren S. R., Skillman E., Ott J., Koribalski B., 2013, ApJ, 765, 136
Tepper-García T., Bland-Hawthorn J., Sutherland R. S., 2015, ApJ, 813, 94
Trachternach C., de Blok W. J. G., Walter F., Brinks E., Kennicutt R. C., Jr, 2008, AJ, 136, 2720
Tully R. B., Rizzi L., Shaya E. J., Courtois H. M., Makarov D. I., Jacobs B. A., 2009, AJ, 138, 323
van der Kruit P. C., Searle L., 1981, A&A, 95, 105
van der Marel R. P., Franx M., 1993, ApJ, 407, 525
Walter F., Brinks E., de Blok W. J. G., Bigiel F., Kennicutt R. C., Jr, Thornley M. D., Leroy A., 2008, AJ, 136, 2563
Yoon J. H., Putman M. E., 2013, ApJ, 772, L29

This paper has been typeset from a TEX/LATEX file prepared by the author.

Downloaded from https://academic.oup.com/mnras/article/469/3/3564/3779716 by Access provided by HEAL-Link (University of Athens) user on 12 December 2022